Preprints (www.preprints.org) | NOT PEER-REVIEWED | Posted: 27 May 2019 doi:10.20944/preprints201905.0316.v1

Article

A new form of velocity distribution in rectangular microchannels with finite aspect ratios

Navid Kashaninejad [1,*]

[1] Queensland Micro- and Nanotechnology Centre, Griffith University, Nathan Campus, QLD 4111 (Australia); navid.kashaninejad@gmail.com

* Correspondence: navid.kashaninejad@gmail.com; Tel.: +61 414 291 080

Received: date; Accepted: date; Published: date

Abstract: This study presents a new form of velocity distribution in laminar liquid flow in rectangular microchannels using the eigenfunction expansion technique. Darcy friction factor and Poiseuille number are also obtained analytically. Due to the symmetry of the solutions, the effects of changing the aspect ratio from 0 to ∞ are also discussed. Using finite element method (FEM), the obtained analytical results are further compared with the 3D numerical simulations for the rectangular microchannels with different range of aspect ratio and pressure gradient, and excellent agreements were found. These findings provide additional insights in interpreting the results of the pressure-driven flows in finite aspect ratio microchannels, in which very precise comparison with the macroscale theory is crucial.

Keywords: Aspect ratio effects; Velocity profile of Poiseuille flow; Friction factor; Eigenfunction expansion technique, Finite element method, 3D microchannels.

---

1. Introduction

Microchannels are basic components in drug delivery devices [1,2], micro-electro-mechanical-systems (MEMS) [3], and lab-on-a-chip systems [4], microfluidic assisted reproductive technology (ART) [5] and other microfluidic components [6-20]. Large surface-to-volume ratio (SVR) [21-23] of microchannels makes them an excellent choice for compact and efficient heat exchangers in electronic cooling devices [24,25]. In biomedical and chemical sciences, microchannels are used to deliver and analyze the micron-sized biological and chemical substances [26-29]. Therefore, a complete understanding of the flow characteristics in microchannels is essential to improve the performance of such an interdisciplinary field.

For fully developed incompressible flow in microchannels at low Reynolds number, partial differential equation (PDE) of the momentum equation simplifies to the classic Poisson equation [30]. Although classical 1D analysis of Hagen-Poiseuille for a cylindrical pipe is usually adapted to solve in noncircular cross-section microchannels by considering the equivalent hydraulic diameter ([31]), analytical modeling for rectangular cross-section microchannels needs 2D analysis ([30),32),33]). Because of the complexity of this approach, most of the previous research works merely focused on high aspect ratio microchannel, which is, in fact, the flow between two parallel plates. One of the drawbacks of such an analysis is that the effect of the side walls is ignored. From the experimental point of view, any discrepancy from the macroscopic theories is related to microscale behavior. This may become misleading if the comparing theories are not very accurate.

The two-dimensional solution of Poisson equation is similar to the theory of elasticity. Therefore, the 2D velocity profile was classically obtained by an analogy with the torsion problem in elasticity using Lagrange stress function [34] and presented by [35] and [36], and well summarized by [37] for different channel cross-sections. In the obtained series solutions for the rectangular channels, the variables of the lateral coordinates were expressed by two different functions, i.e., one variable with hyperbolic function and the other one with trigonometric function. Spiga and Morino used finite Fourier transform to find the velocity profile of the rectangular channels and verified their results by comparing the obtained friction factors with those presented in the literature [33]. Additionally, approximate solutions for the channels by considering the side walls effect also exist. Knowing the maximum velocity, Purday proposed an approximate expression to calculate the average velocity of the channels with the aspect ratio greater than 2 [38]. Using finite difference method for channels with the aspect ratio greater than 3, Natarajan and Lakshmanan presented another approximate solution for the velocity field [39]. Savino and Siegel also suggested an approximate series solution for the channels with the aspect ratio from 1 to ∞ [40]. The other exact series solutions of the Poisson equation were also proposed in the literature [41,42)]. Even though the experimental results verified the accuracy of these models, the convergences of these series solutions were slow and had many computational complexities. Moreover, the lateral coordinates in all, except the solution presented by [33], of these classical solutions of the Poisson equation describing the velocity profile of the finite aspect ratio channels were in the asymmetric form with different numerical exponents. Furthermore, to relate the frictional losses to the average velocity in the channels, classical Darcy-Weisbach equation is used. Subsequently, instead of performing detailed analytical solutions, most commonly, friction factor and Poiseuille number are multiplied by empirical Hartnett–Kostic correction factor to take into account the effect of the microchannels aspect ratio in the literature (see for example a review article by Dey et al. [43]).

In the present paper, a new form of velocity distribution in laminar liquid flow in rectangular microchannels is obtained by adopting the eigenfunction expansion technique [44]. Darcy friction factor and Poiseuille number are also found analytically and the effects of changing the aspect ratio from 0 to ∞ are discussed. Using finite element method (FEM), the obtained analytical results are further compared with the numerical simulations of COMSOL Multiphysics for microchannels with different values of aspect ratio and pressure gradient.

2. Materials and Methods

2.1 Analytical Modeling

In the present study, the velocity distributions of a creeping flow in a rectangular microchannel are derived. This type of flow is dominant at small length scale, low velocity or for a very viscous fluid. By considering hydrophilic channel walls, the boundary conditions (BCs) are the homogeneous no-slip Dirichlet BCs. Yet, the governing equation is still non-homogeneous and the classical method of separation of variables cannot be applied.

In order to solve this type of PDE, the method of eigenfunction expansion can be used, corresponding to the homogeneous BCs and non-homogeneous linear governing PDE equation [44]. It is common in the literature that the origin of coordinates describing the velocity distribution is chosen at the center of the channel (Figure 1-a) but it is mathematically more convenient to transform it to the bottom corner of the channel, (Figure 1-c). The new coordinates X and Y can be defined: $X = x + w$; $Y = y + h$.

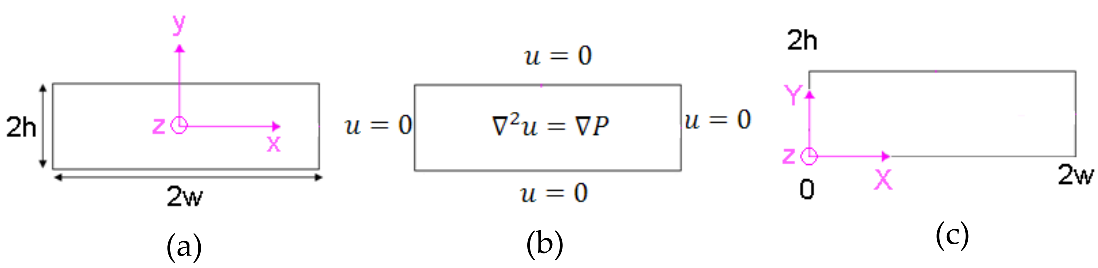

Figure 1. Schematic of the model: a) Rectangular cross-section of the channel with the flow velocity at z-direction (normal to the page). b) Corresponding BCs (no-slip) at the walls and Stokes governing equation; c) Transformation of the coordinate to X and Y

 doi:10.20944/preprints201905.0316.v1

The momentum equation in the streamwise direction becomes:

$$\frac{\partial^2 u}{\partial X^2} + \frac{\partial^2 u}{\partial Y^2} = \frac{\frac{\partial P}{\partial z}}{\mu_w} = F \qquad (1)$$

where u and $\frac{\partial P}{\partial z}$ are the velocity and pressure gradient in the streamwise direction z, respectively. Since $\frac{\partial P}{\partial z}$ and fluid viscosity, μ_w, are constant across the channel cross-section, we denote them with a single variable F. Thus, we need to solve Eq.(1) subject to the following no-slip BCs:

$$BC's \begin{cases} u(0,Y) = 0 \quad ; \qquad u(2w,Y) = 0 \\ u(X,0) = 0 \quad ; \qquad u(X,2h) = 0 \end{cases} \qquad (2)$$

If we can find a function (say, ψ) by which the Laplacian operator is simplified to the operation, i.e., $\nabla^2(\psi) = \lambda.\psi$, then we can find the solution of the problem easily. In mathematical terminology, such function is called eigenfunction with the corresponding λ as the eigenvalue. Eigenfunction should also satisfy the BCs. Accordingly, 2D form of the solution can be written as:

$$u(X,Y) = \sum_{n=1}^{\infty}\sum_{m=1}^{\infty} A_{mn}\, sin(\frac{m\pi}{2w}X)\ sin(\frac{n\pi}{2h}Y) \qquad (3)$$

where A_{mn} is a constant needed to be determined. Substituting this form of the solution into Eq. (1) results:

$$\sum_{n=1}^{\infty}\sum_{m=1}^{\infty} -A_{mn}\left\{\left(\frac{m\pi}{2w}\right)^2 + \left(\frac{n\pi}{2h}\right)^2\right\} sin(\frac{m\pi}{2w}X)\ sin(\frac{n\pi}{2h}Y) = F \qquad (4)$$

Considering the above equation as the double Fourier sinusoidal series expansion of F, we can find the as-yet unknown A_{mn} after some mathematical manipulations:

$$A_{mn} = \frac{-16\ F\ \alpha^2\ h^2}{\{(m\pi)^2 + (\alpha n\pi)^2\}}\left(\frac{1}{m\pi}\right)\left(\frac{1}{n\pi}\right)[1 - cos\ m\pi][1 - cos\ n\pi] \qquad (5)$$

where α is the aspect ratio of the channel, that is:

$$\alpha = \frac{2w}{2h} \qquad (6)$$

By substituting Eq. (5) into Eq. (3), and replacing the (X, Y) with the original (x, y) the final form of the velocity profile becomes:

$$u(x,y) = \frac{-16\ F\ \alpha^2\ h^2}{\pi^4}\sum_{n=1}^{\infty}\sum_{m=1}^{\infty}\frac{[1 - cos\ m\pi][1 - cos\ n\pi]}{m\ n\ (m^2 + \alpha^2 n^2)} sin\frac{m\pi}{2h}(x+w)\ sin\frac{n\pi}{2h}(y+h) \qquad (7)$$

By introducing the normalized velocity u^* :

$$u^*(x,y) = \frac{u(x,y)}{\left(-\frac{\partial P}{\partial z}\right)\ h^2/\mu_w} = \frac{u(x,y)}{-Fh^2} \qquad (8)$$

The final dimensionless form of the velocity becomes:

$$u^*(x,y) = \frac{16\ \alpha^2}{\pi^4}\sum_{n=1}^{\infty}\sum_{m=1}^{\infty}\frac{[1 - cos\ m\pi][1 - cos\ n\pi]}{m\ n\ (m^2 + \alpha^2 n^2)} sin\frac{m\pi}{2\alpha h}(x+w)\ sin\frac{n\pi}{2h}(y+h) \qquad (9)$$

 doi:10.20944/preprints201905.0316.v1

Also the flow rate can be calculated by integrating the velocity distribution, Eq. (7), as:

$$Q = \int_{-h}^{h}\int_{-w}^{w} u(x,y)dx\,dy = \frac{64\left(-\frac{\partial P}{\partial z}\right)\ \alpha^3\ h^4}{\mu_w\, \pi^6}\sum_{n=1}^{\infty}\sum_{m=1}^{\infty}\frac{[1-\cos m\pi]^2[1-\cos n\pi]^2}{m^2\, n^2\,(m^2+\,\alpha^2 n^2)} \qquad (10)$$

Furthermore, the average velocity can be calculated as:

$$Q = \bar{u}\times A \Rightarrow \bar{u} = \frac{Q}{4\,\alpha h^2} \qquad (11)$$

By substituting Eq. (10) into Eq. (11), and some mathematical manipulations, the final form of the average velocity of the channel by considering the aspect ratio effect becomes:

$$\bar{u} = \bar{u}_{H-P}\,\phi(\alpha) \qquad (12)$$

where $\bar{u}_{H-P}$ is the classical Hagen-Poiseuille average velocity:

$$\bar{u}_{H-P} = \frac{h^2}{3\mu_w}\left(-\frac{\partial P}{\partial z}\right) \qquad (13)$$

And $\phi(\alpha)$ is the additional term due to the side walls effects:

$$\phi(\alpha) = \frac{48\alpha^2}{\pi^6}\sum_{n=1}^{\infty}\sum_{m=1}^{\infty}\frac{[1-\cos m\pi]^2[1-\cos n\pi]^2}{m^2\, n^2\,(m^2+\,\alpha^2 n^2)} \qquad (14)$$

Furthermore, Darcy friction factor f can be written as:

$$f = \frac{\left(-\frac{\partial P}{\partial z}\right).{D_h}^2}{\frac{1}{2}\mu_w \bar{u}}\times\frac{1}{Re} \qquad (15)$$

where hydraulic diameter D_h is:

$$D_h = \frac{4(2h.2w)}{2(2h+2w)} = \frac{4\alpha h}{\alpha+1} \qquad (16)$$

By substituting Eq. (12) and Eq. (16) into Eq. (15), Final form of the friction factor becomes:

$$f = \frac{2\,\pi^6}{\sum_{n=1}^{\infty}\sum_{m=1}^{\infty}\frac{[1-\cos m\pi]^2[1-\cos n\pi]^2}{m^2\, n^2\,(m^2+\,\alpha^2 n^2)}\ (\alpha+1)^2}\frac{1}{Re} \qquad (17)$$

Equivalently, we can also define Poiseuille number, Po, by multiplying Darcy friction factor to Reynolds number:

$$Po = 96\,\eta(\alpha) \qquad (18)$$

where:

$$\eta(\alpha) = \frac{\pi^6}{48\,(\alpha+1)^2\sum_{n=1}^{\infty}\sum_{m=1}^{\infty}\frac{[1-\cos m\pi]^2[1-\cos n\pi]^2}{m^2\, n^2\,(m^2+\,\alpha^2 n^2)}} \qquad (19)$$

2.2 Numerical Simulation

 doi:10.20944/preprints201905.0316.v1

To numerically simulate the flow in the rectangular microchannel and validate the results of the theoretical ones, COMSOL Multiphysics 3.5a was used which implements the FEM approach to discretize and solve the governing equations. To this aim, first 3D models of the microchannels with the geometrical sizes shown in Table 1 were sketched:

Table 1. Geometrical sizes of the microchannels used for numerical simulation

$2h\ (\mu m)$	$2w\ (\mu m)$	$L\ (mm)$	$\alpha = w/h$	$D_h\ (\mu m)$
20	60,10	1	3,0.5	30, 13

Subsequently, DI water with a density of $\rho = 1000\ \frac{\text{kg}}{\text{m}^3}$, dynamic viscosity of $\mu_w = 0.001\ \text{Pa.s}$, and zero body forces were defined. Inlet pressure was varied from 500 Pa to 4000 Pa while atmospheric pressure was defined as the outlet BC. Other domains of the microchannel were considered as the solid walls with no-slip BCs.

Total element numbers of 17191 tetrahedral grids were generated after testing the grid independency. The grid shapes, as well as velocity distributions on z-plane, are shown in Figure 2(a,b). 3D form of the Navier-Stokes equation was used to simulate the results.

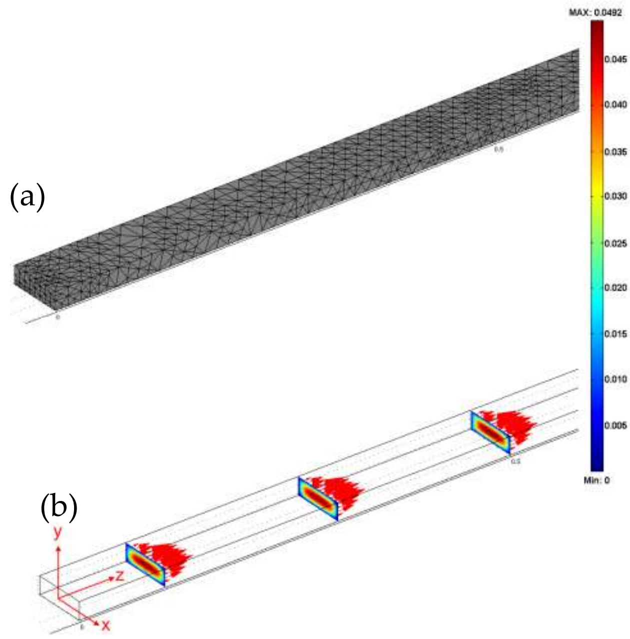

Figure 2. Numerical modeling of the microchannels: (a) Extra fine tetrahedral meshes structures. (b) Numerical velocity distribution on z-plane for pressure gradient of 500 Pa.

3. Results and Discussion

Figure 3 illustrates the variations of the normalized velocity distribution with respect to the aspect ratio, i.e. Eq. (9). The results show that by increasing the aspect ratio, velocity profile becomes more parabolic and the effects of side walls on velocity distributions become negligible. That means, the classical Hagen-Poiseuille equation is the limiting case of the obtained 2D analytical formula when aspect ratio approaches infinity.

Preprints (www.preprints.org) | NOT PEER-REVIEWED | Posted: 27 May 2019 doi:10.20944/preprints201905.0316.v1

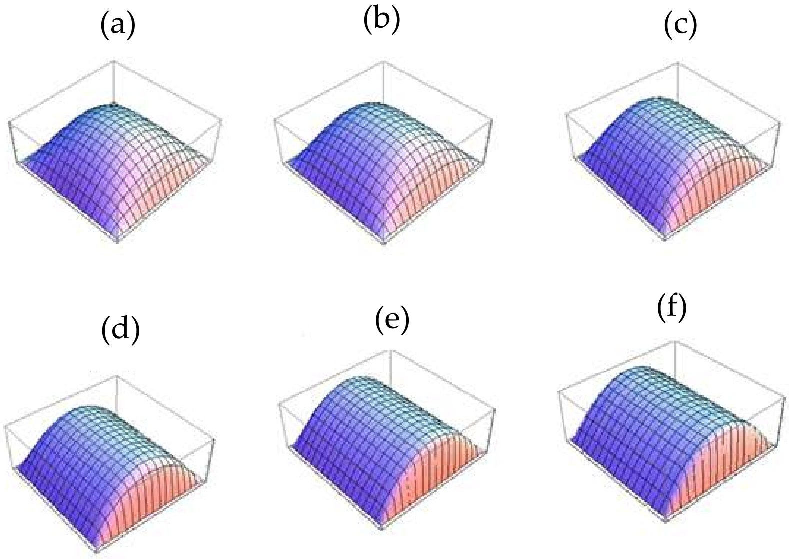

Figure 3. Variations of the normalized velocity (Eq. (9)) at different values of aspect ratio: (a) $\boldsymbol{\alpha} = \mathbf{1}$; (b) $\boldsymbol{\alpha} = \mathbf{3}$; (c) $\boldsymbol{\alpha} = \mathbf{5}$; (d) $\boldsymbol{\alpha} = \mathbf{10}$; (e) $\boldsymbol{\alpha} = \mathbf{20}$; (f) $\boldsymbol{\alpha} = \mathbf{30}$;

To further illustrate the effect of aspect ratio on frictional losses, Poiseuille number is plotted as a function of aspect ratio in Figure 4. Two distinctive cases are distinguishable. First, when the aspect ratio is less than unity (lower left inset of Figure 4). In this case, Poiseuille number increases by decreasing the aspect ratio. In the limiting case of zero aspect ratio, it approaches up to 96. Second situation, corresponds to the case where aspect ratio is more than unity (upper right inset of Figure 4). In that case, Poiseuille number increases by increasing the aspect ratio. Consistently, for very large aspect ratio, maximum value of Poiseuille number becomes 96 corresponding to the two parallel plates channels. Generally, it can be concluded for the laminar flow at the same Reynolds number, square cross-section channels ($\alpha = 1$) generates the lowest frictional losses and as the channel cross-section deviates from being square shape, frictional losses increases (up to 74%).

 doi:10.20944/preprints201905.0316.v1

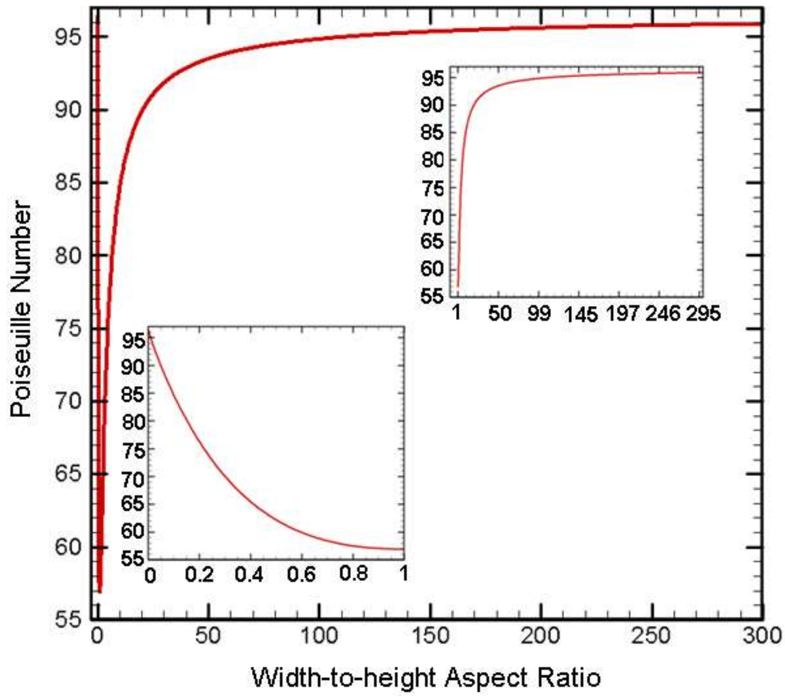

Figure 4. Poiseuille number $\mathbf{Po}$ vs. aspect ratio $\boldsymbol{\alpha}$. The insets at the lower left and upper right show Po variations for $\mathbf{0} < \boldsymbol{\alpha} < \mathbf{1}$ and $\boldsymbol{\alpha} \geq \mathbf{1}$, respectively.

Comparison between the derived analytical velocity distributions, i.e., Eq. (7), and the obtained numerical results across the channel height and width (along the vertical and horizontal directions of the microchannel, respectively) are illustrated in Figure 5 for two different values of channel aspect ratio at the same pressure gradient (500Pa). The analytical results are in excellent agreement with the numerical simulations at different locations of the channel cross-section. As expected, maximum velocity occurs at the midplanes ($x = y = 0$). Also, it is shown that the classical equation of Hagen-Poiseuille, i.e. Eq. (13), can only predict the maximum velocity distributions on the midplane, i.e. $x = 0$ for $\alpha > 1$ and $y = 0$ for $\alpha < 1$. Further, this equation overestimates the numerical and 2D velocity values.

Figure 5(a) also indicates that on the plane at $2\mu m$ near to the side walls of the channel, i.e., $x = 28\mu m$, the numerical results are notably less than the analytical ones. In particular, maximum values of velocity are 4.51mm/s and 6.48mm/s corresponding to the numerical and analytical results, respectively. In this case, analytical maximum velocity is 30% higher compared to the numerical one.

Preprints (www.preprints.org) | NOT PEER-REVIEWED | Posted: 27 May 2019 doi:10.20944/preprints201905.0316.v1

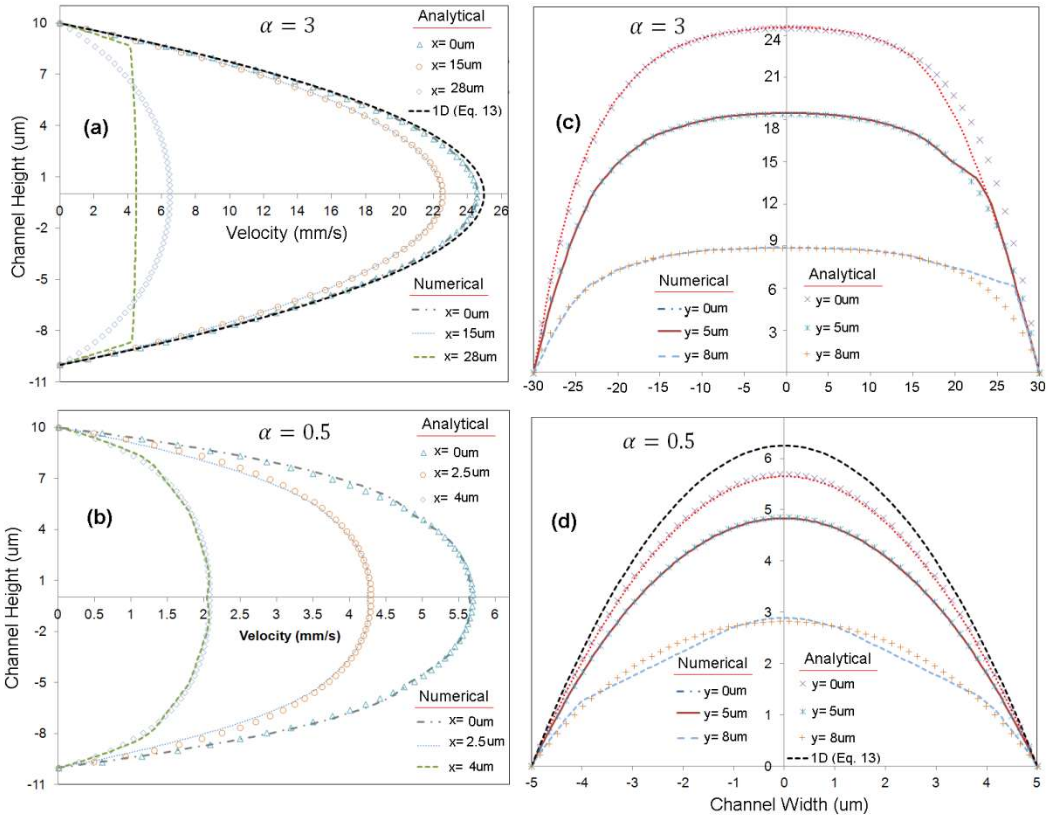

Figure 5. Velocity distributions at different channel positions and aspect ratios (P=500Pa) as compared with the obtained analytical formula and numerical results. (a), (b) Velocity profiles across the channel height. (c), (d) Velocity profiles across the channel width

This observation is consistent with the experimental observation of [45] who used micro-particle image velocimetry (micro-PIV) to probe the velocity distribution of DI water at different microchannel locations with an aspect ratio of 2.8. They found that very near the hydrophilic wall, the measured velocities were significantly larger than the theoretical velocity. Therefore, the larger values of analytical velocity presented in this study is closer to the experimental observations in the literature.

4. Conclusions

In this study, classical Hagen-Poiseuille and Darcy-Weisbach equations were modified by introducing the effect of the aspect ratio of the rectangular microchannels. Compared to the previous 2D exact solutions, the present series solutions were symmetrical (x and y lateral coordinates are interchangeable) and converged very fast (owing to the 3rd and 4th powers of the computational indexes, i.e. m and n, in the denominator of the formulae, c.f., Eq. (7) or Eq. (14)). In addition, the obtained exact solutions are valid for any range of the channel aspect ratio. It was also shown that 1D classical equations were the limiting cases of the obtained 2D analytical formulae for velocity distributions and friction factor when the channel aspect ratio approached infinity. The results also indicated that for the laminar flow at the same Reynolds number, square cross-section channels ($\alpha = 1$) generated the lowest frictional losses. As the channel cross-section deviated from the square shape, the Poiseuille number increased significantly from 55 (square section) to 96 (parallel plates). Moreover, the obtained analytical formula was compared with the numerical simulations of the 3D pressure driven laminar flow in rectangular microchannels with hydraulic diameters of $13\mu m$ and $30\mu m$, and excellent agreements were found even for on the plane very close to the microchannel top wall. On the plane at $2\mu m$ near to the side walls of the microchannel with larger aspect ratio larger than unity, i.e. $\alpha = 3.0$, analytical maximum velocity was 30% higher compared to the numerical one which was consistent with the experimental micro-PIV results in the literature for the similar microchannel. Although the obtained results are applicable to any rectangular ducts, they are more useful in interpreting the pressure-driven flows in microchannels, in which very careful comparison is crucial in interpreting the results.

Conflicts of Interest: The author declares no conflict of interest

References

1. Nguyen, N.-T.; Shaegh, S.A.M.; Kashaninejad, N.; Phan, D.-T. Design, fabrication and characterization of drug delivery systems based on lab-on-a-chip technology. *Advanced Drug Delivery Reviews* **2013**, *65*, 1403-1419, doi:https://doi.org/10.1016/j.addr.2013.05.008.
2. Moghadas, H.; Saidi, M.S.; Kashaninejad, N.; Nguyen, N.-T. Challenge in particle delivery to cells in a microfluidic device. *Drug Delivery and Translational Research* **2018**, *8*, 830-842, doi:10.1007/s13346-017-0467-3.
3. Dinh, T.; Phan, H.-P.; Kashaninejad, N.; Nguyen, T.-K.; Dao, D.V.; Nguyen, N.-T. An On-Chip SiC MEMS Device with Integrated Heating, Sensing, and Microfluidic Cooling Systems. *Advanced Materials Interfaces* **2018**, *5*, 1800764, doi:10.1002/admi.201800764.
4. Gerami, A.; Alzahid, Y.; Mostaghimi, P.; Kashaninejad, N.; Kazemifar, F.; Amirian, T.; Mosavat, N.; Ebrahimi Warkiani, M.; Armstrong, R.T. Microfluidics for Porous Systems: Fabrication, Microscopy and Applications. *Transport in Porous Media* **2018**, 10.1007/s11242-018-1202-3, doi:10.1007/s11242-018-1202-3.
5. Kashaninejad, N.; Shiddiky, M.J.A.; Nguyen, N.-T. Advances in Microfluidics-Based Assisted Reproductive Technology: From Sperm Sorter to Reproductive System-on-a-Chip. *Advanced Biosystems* **2018**, *2*, 1700197, doi:10.1002/adbi.201700197.
6. Barisam, M.; Saidi, S.M.; Kashaninejad, N.; Nguyen, N.-T. Prediction of Necrotic Core and Hypoxic Zone of Multicellular Spheroids in a Microbioreactor with a U-Shaped Barrier. *Micromachines* **2018**, *9*, doi:10.3390/mi9030094.
7. Barisam, M.; Saidi, S.M.; Kashaninejad, N.; Vadivelu, R.; Nguyen, N.-T. Numerical Simulation of the Behavior of Toroidal and Spheroidal Multicellular Aggregates in Microfluidic Devices with Microwell and U-Shaped Barrier. *Micromachines* **2017**, *8*, doi:10.3390/mi8120358.
8. Kashaninejad, N.; Nguyen, N.-T.; Chan, W.K. Eccentricity effects of microhole arrays on drag reduction efficiency of microchannels with a hydrophobic wall. *Physics of Fluids* **2012**, *24*, 112004, doi:10.1063/1.4767539.
9. Kashaninejad, N.; Nguyen, N.-T.; Chan, W.K. The three-phase contact line shape and eccentricity effect of anisotropic wetting on hydrophobic surfaces. *Soft Matter* **2013**, *9*, 527-535, doi:10.1039/C2SM26963E.
10. Maleki, M.A.; Soltani, M.; Kashaninejad, N.; Nguyen, N.-T. Effects of magnetic nanoparticles on mixing in droplet-based microfluidics. *Physics of Fluids* **2019**, *31*, 032001, doi:10.1063/1.5086867.
11. Moghadas, H.; Saidi, M.S.; Kashaninejad, N.; Kiyoumarsioskouei, A.; Nguyen, N.-T. Fabrication and characterization of low-cost, bead-free, durable and hydrophobic electrospun membrane for 3D cell culture. *Biomedical Microdevices* **2017**, *19*, 74, doi:10.1007/s10544-017-0215-y.

12. Moghadas, H.; Saidi, M.S.; Kashaninejad, N.; Nguyen, N.-T. A high-performance polydimethylsiloxane electrospun membrane for cell culture in lab-on-a-chip. *Biomicrofluidics* **2018**, *12*, 024117, doi:10.1063/1.5021002.
13. Moshksayan, K.; Kashaninejad, N.; Saidi, M. Numerical investigation of the effects of functional parameters in hypoxia initiation within a cell spheroid cultured in a microfluidic chip. In Proceedings of Proceedings of the 25th Annual International Conference on Mechanical Engineering held by ISME, Tehran, Iran; pp. 2-4.
14. Moshksayan, K.; Kashaninejad, N.; Saidi, S.M. Inventions and Innovations in Preclinical Platforms for Cancer Research. *Inventions* **2018**, *3*, doi:10.3390/inventions3030043.
15. Nguyen, N.-T.; Hejazian, M.; Ooi, H.C.; Kashaninejad, N. Recent Advances and Future Perspectives on Microfluidic Liquid Handling. *Micromachines* **2017**, *8*, doi:10.3390/mi8060186.
16. Rismanian, M.; Saidi, M.S.; Kashaninejad, N. A new non-dimensional parameter to obtain the minimum mixing length in tree-like concentration gradient generators. *Chemical Engineering Science* **2019**, *195*, 120-126, doi:https://doi.org/10.1016/j.ces.2018.11.041.
17. Rostami, P.; Kashaninejad, N.; Moshksayan, K.; Saidi, M.S.; Firoozabadi, B.; Nguyen, N.-T. Novel approaches in cancer management with circulating tumor cell clusters. *Journal of Science: Advanced Materials and Devices* **2019**, *4*, 1-18, doi:https://doi.org/10.1016/j.jsamd.2019.01.006.
18. Tajik, P.; Saidi, M.S.; Kashaninejad, N.; Nguyen, N.-T. Simple, Cost-Effective, and Continuous 3D Dielectrophoretic Microchip for Concentration and Separation of Bioparticles. *Industrial & Engineering Chemistry Research* **2019**, 10.1021/acs.iecr.9b00771, doi:10.1021/acs.iecr.9b00771.
19. Vadivelu, R.; Kashaninejad, N.; Sreejith, K.R.; Bhattacharjee, R.; Cock, I.; Nguyen, N.-T. Cryoprotectant-Free Freezing of Cells Using Liquid Marbles Filled with Hydrogel. *ACS Applied Materials & Interfaces* **2018**, *10*, 43439-43449, doi:10.1021/acsami.8b16236.
20. Yadav, S.; Kashaninejad, N.; Masud, M.K.; Yamauchi, Y.; Nguyen, N.-T.; Shiddiky, M.J.A. Autoantibodies as diagnostic and prognostic cancer biomarker: Detection techniques and approaches. *Biosensors and Bioelectronics* **2019**, *139*, 111315, doi:https://doi.org/10.1016/j.bios.2019.111315.
21. Kashaninejad, N.; Chan, W.K.; Nguyen, N.-T. Fluid Mechanics of Flow Through Rectangular Hydrophobic Microchannels. *ASME 2011 9th International Conference on Nanochannels, Microchannels, and Minichannels* **2011**, *1*, 647-655, doi:10.1115/ICNMM2011-58140.
22. Kashaninejad, N.; Chan, W.K.; Nguyen, N.-T. Eccentricity Effect of Micropatterned Surface on Contact Angle. *Langmuir* **2012**, *28*, 4793-4799, doi:10.1021/la300416x.
23. Kashaninejad, N.; Kong Chan, W.; Nguyen, N.-T. Analytical Modeling of Slip Flow in Parallel-plate Microchannels. *Micro and Nanosystems* **2013**, *5*, 245-252.
24. Nguyen, N.; Wereley, S. *Fundamentals and applications of microfluidics*; Artech House Publishers: 2002.
25. Tabeling, P. *Introduction to microfluidics*; Oxford University Press, USA: 2005.
26. Zhao, C.; Lu, T. Analysis of microchannel heat sinks for electronics cooling. *International Journal of Heat and Mass Transfer* **2002**, *45*, 4857-4869.
27. Morini, G.L. Single-phase convective heat transfer in microchannels: a review of experimental results. *International Journal of Thermal Sciences* **2004**, *43*, 631-651.
28. Kashaninejad, N.; Nikmaneshi, R.M.; Moghadas, H.; Kiyoumarsi Oskouei, A.; Rismanian, M.; Barisam, M.; Saidi, S.M.; Firoozabadi, B. Organ-Tumor-on-a-Chip for Chemosensitivity Assay: A Critical Review. *Micromachines* **2016**, *7*, doi:10.3390/mi7080130.

29. Moshksayan, K.; Kashaninejad, N.; Warkiani, M.E.; Lock, J.G.; Moghadas, H.; Firoozabadi, B.; Saidi, M.S.; Nguyen, N.-T. Spheroids-on-a-chip: Recent advances and design considerations in microfluidic platforms for spheroid formation and culture. *Sensors and Actuators B: Chemical* **2018**, *263*, 151-176, doi:https://doi.org/10.1016/j.snb.2018.01.223.
30. White, F.M. *Viscous fluid flow*; McGraw-Hill New York: 1991; Vol. 2.
31. Sutera, S.P.; Skalak, R. The history of Poiseuille's law. *Annual Review of Fluid Mechanics* **1993**, *25*, 1-20.
32. Shah, R.K.; London, A.L. *Laminar flow forced convection in ducts: a source book for compact heat exchanger analytical data*; Academic press New York: 1978.
33. Spiga, M.; Morino, G.L. A symmetric solution for velocity profile in laminar flow through rectangular ducts. *International Communications in Heat and Mass Transfer* **1994**, *21*, 469-475, doi:10.1016/0735-1933(94)90046-9.
34. Timoshenko, S.P.; Goodier, J.N. Theory of elasticity. McGraw-Hill, New York: 1970.
35. Knudsen, J.G.; Katz, D.L. *Fluid dynamics and heat transfer*; McGraw-Hill New York: 1958; Vol. 101.
36. Berker, R. Handbook of fluid dynamics, vol. VIII/3. Springer, Berlin: 1963.
37. Wang, C. Exact solutions of the steady-state Navier-Stokes equations. *Annual Review of Fluid Mechanics* **1991**, *23*, 159-177.
38. Purday, H. An introduction to the mechanics of viscous flow. *Dover, New York* **1949**.
39. Natarajan, N.; Lakshmanan, S. Laminar Flow in rectangular ducts: prediction of velocity profiles and friction factor. *Indian J. Technol* **1972**, *10*, 435-438.
40. Savino, J.M.; Siegel, R. Laminar forced convection in rectangular channels with unequal heat addition on adjacent sides. *International Journal of Heat and Mass Transfer* **1964**, *7*, 733-741, doi:10.1016/0017-9310(64)90004-3.
41. Holmes, D.; Vermeulen, J. Velocity profiles in ducts with rectangular cross sections. *Chemical Engineering Science* **1968**, *23*, 717-722.
42. Sparrow, E.M.; Hixon, C.; Shavit, G. Experiments on laminar flow development in rectangular ducts. *Journal of Basic Engineering* **1967**, *89*, 116.
43. Dey, R.; Das, T.; Chakraborty, S. Frictional and heat transfer characteristics of single-phase microchannel liquid flows. *Heat Transfer Engineering* **2012**, *33*, 425-446.
44. Asmar, N. Partial differential equations and boundary value problems with fourier series. *Prentice Hall* **2005**, *second edition*.
45. Zheng, X.; Silber-Li, Z. Measurement of velocity profiles in a rectangular microchannel with aspect ratio = 0.35. *Experiments in Fluids* **2008**, *44*, 951-959.